Gate control of carrier distribution in *k*-space in MoS_2 monolayer and bilayer crystals

Tilmar Kümmell,* Wolf Quitsch, Sebastian Matthis, Tobias Litwin, and Gerd Bacher
Werkstoffe der Elektrotechnik and CENIDE, Universität Duisburg-Essen, Bismarckstraße 81, 47057 Duisburg, Germany
(Received 6 November 2014; revised manuscript received 25 February 2015; published 17 March 2015)

We demonstrate gate control of the carrier distribution in *k*-space in bilayer and monolayer MoS_2 devices, probed by microphotoluminescence spectroscopy on a contacted single flake. The characteristic emission lines of the neutral and the negatively charged exciton act as a sensor for electron depletion/agglomeration via gate voltage. Gate-induced carrier depletion enhances the sensitivity to defects in monolayers, whereas in bilayers the indirect transition becomes more weight. The specific band structure of bilayers results in a thermal dissociation of trions at 200 K and above, in contrast to monolayers where trion emission is observed up to room temperature. We show that these findings are a consequence of a bias-driven redistribution of charge carriers between the different band minima.

DOI: 10.1103/PhysRevB.91.125305 PACS number(s): 78.55.Hx, 78.66.Li, 71.35.Pq, 71.20.Nr

I. INTRODUCTION

Two-dimensional (2D) transition-metal chalcogenides (TMCs) have recently shifted into the focus of nanomaterial science [1,2]. Similar to graphene, flakes consisting of one or few monolayers can be easily realized by mechanical exfoliation. Although subnanometer thickness is attractive for ultrathin flexible electronics [3] or light-emitting devices [4–6], it has turned out that monolayers from, e.g., MoS_2, $MoSe_2$, or WSe_2, exhibit a unique band structure that could evoke new components for spintronics or valleytronics [7–15]. Whereas the corresponding bulk materials are indirect semiconductors, monolayer crystals exhibit a direct band gap, leading to strong photoluminescence after optical excitation. In between, a more or less gradual change from a direct to an indirect semiconductor is expected with growing layer number [16–18]. In ultrathin TMCs, such as MoS_2, the direct transition occurs at the K point of the Brillouin zone and is nearly independent of layer thickness [2]. In contrast, the indirect transition is expected to depend strongly on the number of layers.

One important reason for the high interest in ultrathin TMCs is the manifold of approaches to manipulate this rich band structure and in particular the carrier population of the corresponding band extrema according to the requirements in possible applications. For instance, the feasibility for light-emitting devices can be enhanced by suppressing the luminescence of the indirect transition. Different strategies for band-structure tuning have been evaluated. Both temperature [19] and strain variation [20–23] can modify the direct and indirect band-gaps' sizes and thus the intensity ratio between indirect and direct transition in luminescence measurements. Most attractive, however, should be a manipulation by electrical signals as these can be applied in a fast and reversible way. Gate voltages have been discussed as a tool for manipulating the valley magnetic moments of the carriers, giving promising perspectives for using the valley polarization as a degree of freedom [11,15]. Generally, electrically contacted flakes show a strong impact on the carrier population in the respective conduction- and valence-band minima on the photoluminescence. By electron injection, MoS_2 flakes can be negatively doped, shifting the Fermi energy into the conduction band up to a level where a transition to a degenerate semiconductor occurs. This technique has been exploited frequently to realize ultrathin transistors using a back gate to control the conductivity in the flakes [24,25]. Moreover, in recent work it has been shown that this carrier injection can be monitored optically by observing charged excitons in photoluminescence [26]. In monolayers the carriers are concentrated at the K minimum of the conduction band. In bilayers with their more complex band structure and their recombination channels via direct *and* indirect transitions, this technique of controlled carrier population should provide a flexible tuning knob for distributing the carriers in the *k*-space. In addition, a direct influence of electric fields on the band gap in bilayer and few-layer structures due to the giant Stark effect has been predicted by theory recently in a number of papers [27–30]. To exploit the potential of real mono- and few-layer TMC-based devices, the interplay between field effects—such as inversion symmetry breaking [11,15] or Stark shift—and carrier population has to be clarified.

In this paper, we use combined optical and electrical carrier injection to populate conduction- and valence-band minima of MoS_2 mono- and bilayer crystal devices in a deterministic way. We demonstrate gate control of the carrier population in *k*-space with a pronounced difference for monolayer and bilayer devices caused by the characteristic thickness-dependent band structure. We show that the optical transitions in the devices are hardly influenced by the Stark shift but strongly depend on the carrier population in the different band minima with consequences for both defect luminescence and interplay between direct and indirect transitions.

II. SAMPLES AND SETUP

The structures were fabricated by mechanical exfoliation of MoS_2 on *n*-doped Si substrates that are covered with 90-nm SiO_2. Raman spectroscopy was employed to determine the thickness of the flakes on the substrate and to unambiguously identify mono- and bilayer structures [31,32]. Photoluminescence (PL) measurements were performed in a micro-PL setup. The samples are mounted in a cryostat with electrical feedthroughs. Optical excitation was performed by a frequency doubled solid-state laser with an emission wavelength of $\lambda = 532$ nm. A microscope objective (50×) was used to focus the

*Corresponding author: tilmar.kuemmell@uni-due.de

 ©2015 American Physical Society

laser on the MoS_2 flakes with submicrometer resolution. The luminescence was collected by the same objective, spectrally dispersed in a Jobin-Yvon iHR-550 monochromator, and recorded by a CCD camera.

For a controlled electrical carrier injection, the flakes on the substrates were contacted via strip lines, defined by electron-beam lithography and evaporation of Ti/Au (10-nm/50-nm) contacts. The substrate was mounted on a ceramic carrier with gold contacts using conductive silver; by doing so the substrate serves as a back gate contact.

III. EXPERIMENTAL RESULTS AND DISCUSSION

The PL emission of a monolayer (diameter of $\sim 2\ \mu$m) and a bilayer flake (diameter of $\sim 4\ \mu$m) at $T = 5$ K are compared in Fig. 1. In this case, the flakes are not yet contacted, i.e., this experiment is expected to be dominated by *photogenerated* electrons and holes. As a common feature, we see a strong emission at around 1.9 eV. This emission can be attributed to the direct transition (A line) at the K point of the Brillouin zone and is a typical feature of two-dimensional MoS_2. Strong PL emission from the direct transition is found from the monolayer and as well from the bilayer flake, confirming a prevailing carrier population at the K point even for the bilayer. For both flakes, we detect an emission peak at ~ 2.1 eV as well, belonging to the direct gap B exciton [2]. In the monolayer flake, an additional significant emission is visible at 1.808 eV (denoted as the L line). This emission is often attributed to defect states, dependent on the surrounding, and is a first hint to a strong surface influence in monolayer samples [33,34].

The A transition itself bears valuable information for mono- and bilayers because the emission actually consists of two lines (see Fig. 1). This fine structure can serve as a monitor for additional carriers populating the K point: From absorption measurements in monolayers [26] it is argued that the two components of the A line belong to a neutral exciton A^0 and a negatively charged exciton (trion) A^-. Fitting the monolayer PL spectra with Lorentzian line shapes (shaded areas in Fig. 1), we can clearly separate three maxima at $E(A^0) = 1.921$ eV, $E(A^-) = 1.896$ eV, and $E(L) = 1.808$ eV for the exciton, the trion, and the defect bound exciton, respectively.

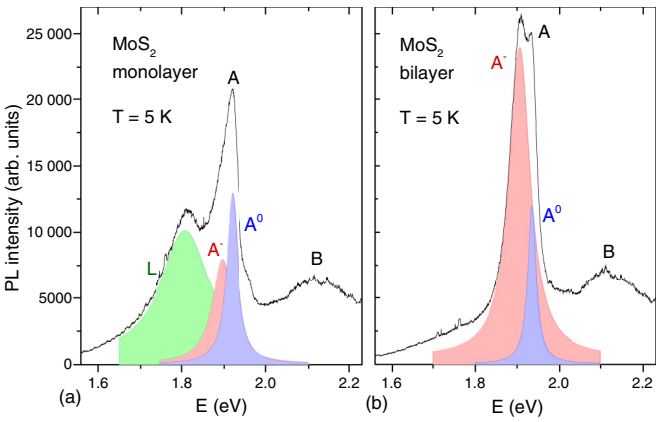

FIG. 1. (Color online) Photoluminescence spectra of the MoS_2 (a, left) monolayer and (b, right) bilayer flakes. The colored curves represent the Lorentzians used for fitting the line shape.

Although this behavior is well known from MoS_2 monolayers, we observe the A^0 and the A^- lines in the MoS_2 bilayer as well. The spectra are clearly separated and the energy difference $\Delta E(A^0 - A^-) = 28$ meV is even slightly larger than observed in monolayer MoS_2. This value is much larger than in usual two-dimensional quantum well heterostructures due to the reduced dielectric screening in 2D materials [35,36] and in good agreement with recent theoretical calculations for monolayers [35], whereas corresponding calculations for bilayers are not yet available. From our fits we extract a trion linewidth of 57 ± 5 meV for both mono- and bilayer MoS_2, clearly exceeding the observed linewidth of the neutral exciton (23 vs 33 meV for bilayer and monolayer MoS_2, respectively). As the trions are generally expected to be larger in diameter [35,37] than the neutral excitons, their enhanced PL linewidth might be attributed to lateral inhomogeneities and local charge fluctuations. This is in agreement with findings that the Stokes shift for trions tends to be larger than for excitons [26].

In order to get an additional knob for controlling the carrier population in conduction and valence bands, exactly the same MoS_2 flakes as discussed above have been contacted via e-beam lithography. The PL spectra have changed slightly after contacting with respect to the noncontacted flakes even without applied voltage. We attribute this to some amount of negative doping: An electron flow from the Au/Ti contacts to the MoS_2 flakes is expected to occur even without external voltage, considering the work function difference between MoS_2 (5.3 eV [38]) and titanium (4.3 eV). In the following, the contacts at the flakes are set to ground potential and a back gate voltage U_G is applied to the substrate in order to manipulate the Fermi energy E_F and by this the carrier population in the crystal. The gate voltage U_G was varied between -30 and $+30$ V, leading to electron accumulation (depletion) for positive (negative) U_G. It should be noted that due to the thin oxide layer ($d = 90$ nm) relatively low values of U_G are sufficient to achieve the same shifts of E_F as in recent reports that are based on a SiO_2 layer thickness of 280 nm and more [11,26].

In Fig. 2(a), PL spectra of the monolayer sample are depicted for different bias voltages at $T = 5$ K. The luminescence for negative gate voltages is dominated by a very

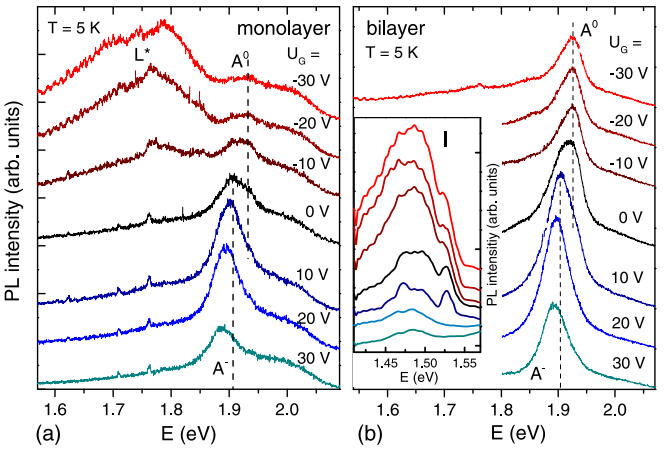

FIG. 2. (Color online) (a) Gate-voltage-dependent PL spectra of the (a) monolayer and the (b) bilayer flakes. In the inset of (b), the indirect transition I has been plotted for different gate voltages.

intense and broad luminescence between 1.6 and 1.8 eV, strongly changing with gate voltage. We want to point out that similar emission in MoS_2 has been seen under bias before [11,12] but not been discussed in detail. In WSe_2 in contrast, a bias-dependent defect emission is found only for bilayers [15] but is absent in the case of monolayer devices [39]. In this low-energy luminescence (denoted as L^*) we find features from the bound exciton (L) before contacting (see Fig. 1) and further maxima at lower energies. It resembles the defect activated luminescence observed by Tongay *et al.* [40], which was attributed to sulfur vacancies activated by charge depletion via electron transfer to surfactant nitrogen molecules in a N_2 atmosphere. In contrast, in our case, charge depletion is induced by the negative gate voltage. At positive gate bias, these defect states become saturated by the injected excess electrons and thus optically inactive. Therefore, the defect luminescence vanishes as can be seen in Fig. 2(a). Note that even at $U_G = 0\,\mathrm{V}$, L^* is not detectable in the contacted flake, whereas L is present in the noncontacted one. This confirms the electron flow from the contact into the flake as mentioned above.

We focus our discussion now on the A emission. Here, an apparent shift to lower energies occurs with rising U_G. This shift shows a discontinuous jump for values between $U_G = -10$ and 10 V, which indicates that it cannot be attributed to a (continuous) field-induced band-gap reduction [28]. It rather indicates a carrier-induced doping of the flake [26]: Increasing the gate voltage from negative to positive values, switching from A^- to A^0 emission occurs at around $U_G = 0\,\mathrm{V}$ as indicated by the dashed vertical lines. This situation at the K point is illustrated in the schematic of the band structure [Fig. 3(a)]: At high positive gate voltage (bottom), the flake is strongly doped with electrons as indicated by a Fermi level located close to or even in the conduction band. After optical generation of electron-hole pairs, these background electrons favor the generation of trions, which

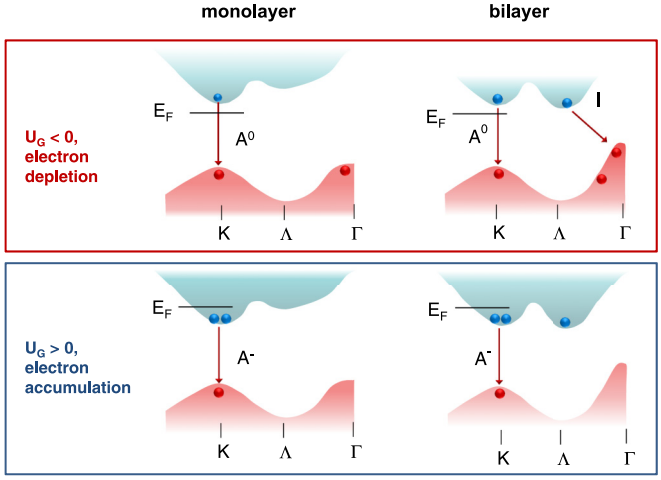

FIG. 3. (Color online) Sketch of the band structures of the mono- and bilayer MoS_2 for different gate voltages U_G. Whereas in the monolayer a switching between an exciton and a negatively charged trion is expected, in the bilayer additional contributions from the indirect transition should be observed for negative gate voltage. Further details can be found in the text.

dominate the emission spectrum as seen in the experiment. With decreasing gate voltage, the Fermi level shifts to lower energies, and the number of excess electrons decreases, thus giving the neutral exciton emission (A^0) more weight.

Whereas the behavior of the monolayer flake with its dominating direct transition described above is principally well understood and discussed in literature for MoS_2 [26] and other two-dimensional semiconductors [13,39], the situation should be different in a MoS_2 bilayer device. Here the modified energy dispersion in the conduction band is expected to impact the optically and electrically injection carrier population within the bands significantly. We focus at first on the K point. In Fig. 2(b), the PL spectra of the bilayer device are plotted for various gate voltages. Similar to what is observed in the monolayer, the charge state should be reflected in the PL signal. Indeed, a clear change in the PL peak position can be observed with decreasing U_G with the pronounced jump in the range between $U_G = 0$ and 10 V. This is again related to the typical switching between the A^0-dominated emission for negative bias and the dominant A^- emission for positive bias. In this light, the observed bias-dependent energy shift observed in MoS_2 bilayers in earlier papers [11,39] might be interpreted as well as an exciton-trion interplay. The broad defect luminescence that was dominating the monolayer spectra for negative bias is practically absent. For $U \leqslant -20\,\mathrm{V}$ only a weak blurred shoulder can be traced at the low-energy side, making the $A^- - A^0$ transition much more clearly visible as compared to the monolayer. This gives some more evidence that the L line is mainly related to a surface effect, which is more pronounced for MoS_2 monolayers than for bilayers.

According to the unique band structure of the bilayer with similar energies for the K- and the Λ-conduction-band minima, we expect an important contribution of the indirect transition I to the luminescence that is known to play a growing role with increasing layer number [2,9]. In the inset of Fig. 2(b), these indirect transition PL spectra are depicted for different gate voltages. Currently there is still a discussion about which local conduction-band minimum is contributing to this indirect transition. Although some earlier papers attributed it to the K point [23,29,41], we follow the models of recent research indicating a predominant involvement of the Λ point [2,9,16,19]. Interestingly, the luminescence of the indirect transition I gains intensity for increasing negative bias, whereas simultaneously the direct transition becomes weaker. At a positive gate voltage $U_G = +30\,\mathrm{V}$, the I emission is hardly detectable, and the direct transition A^- dominates the emission spectrum.

We interpret this finding by considering the bilayer band structure [Fig. 3(b)]: The main difference to the monolayer is the lower energy of the conduction-band valley at the Λ point and the higher energy of the valence-band hill at the Γ point. These two features, which are caused by the gradual change from monolayer to bulk properties, permit in combination the indirect transition between the Λ point in the conduction band and the Γ point in the valence band [2,16,19]. In the case of positive U_G, the conduction band is floated with electrons, and these will populate more than one region in the k-space, i.e., K and Λ points, as predicted in Ref. [17]. Optical excitation will predominantly generate electrons and holes at the K point. Thus, we observe mainly

trions at the K point as discussed before. For negative U_G, the situation is different: In addition to the direct transition (A) we observe now the indirect transition I that gradually increases in the depleting regime. We attribute this to a growing number of holes that will accumulate under negative gate voltage at the valence-band maximum, i.e., at the Γ point. After optical excitation, these holes can recombine with photogenerated electrons in the conduction-band minimum (Λ point). This leads to a strong indirect transition [see Fig. 3(b), top] in addition to the direct transition at the K point. We want to point out that the total intensity (i.e., the sum of I, A^0, and A^-) does not change significantly for $-30\,\mathrm{V} \leqslant U_G \leqslant 20\,\mathrm{V}$. Apparently, the number of holes in the structures plays an important role, controlling the intensity ratio between A and I lines.

All these changes in the PL spectra with gate voltage can be attributed to carrier redistribution in k-space. In Figs. 4(a) and 4(b) we plotted the PL energy maximum in dependence of the gate voltage for the A^0 and A^- lines as extracted from fitting the spectra with Lorentzian functions. It can be seen clearly that for negative gate voltages, no noticeable energy shift can be observed for the A^0 and A lines in both devices, and a small redshift is found for positive U_G. It should be noted that theoretical calculations performed for double-gate architecture expect a significant Stark effect in bilayers, reducing the direct band gap [27–30] and the energy difference between the conduction-band minima and by this the ratio of the direct to indirect transition [30]. In our capacitor geometry, however, the fields acting on the MoS_2 layer are expected to be small, and therefore, the Stark shift should be negligible. The small but continuous redshift for $U_G > 10\,\mathrm{V}$ that we observe for *both* mono- and bilayers is more likely caused by a band-gap renormalization caused by the high electron densities. Using a simple plate capacitor model for the dielectric SiO_2 layer, we estimate a capacitance between the flake and the back gate of $C = 3 \times 10^{-8}\,\mathrm{F/cm^2}$ for our structure. The field effect would result in a gate-voltage-induced change in carrier density of $\Delta n = C \times \Delta U_G/e$, i.e., about $2 \times 10^{11}\,\mathrm{cm^{-2}/V}$. From this, we expect a redshift of several meV due to renormalization effects for a gate bias variation between $U_G = 0$ and 30 V [21]. Thus, our considerations imply that the transition energies of electrically contacted MoS_2 flakes are significantly more influenced by changes in the carrier concentration and their distribution between the band extrema in the conduction and the valence bands than by perpendicular electric fields.

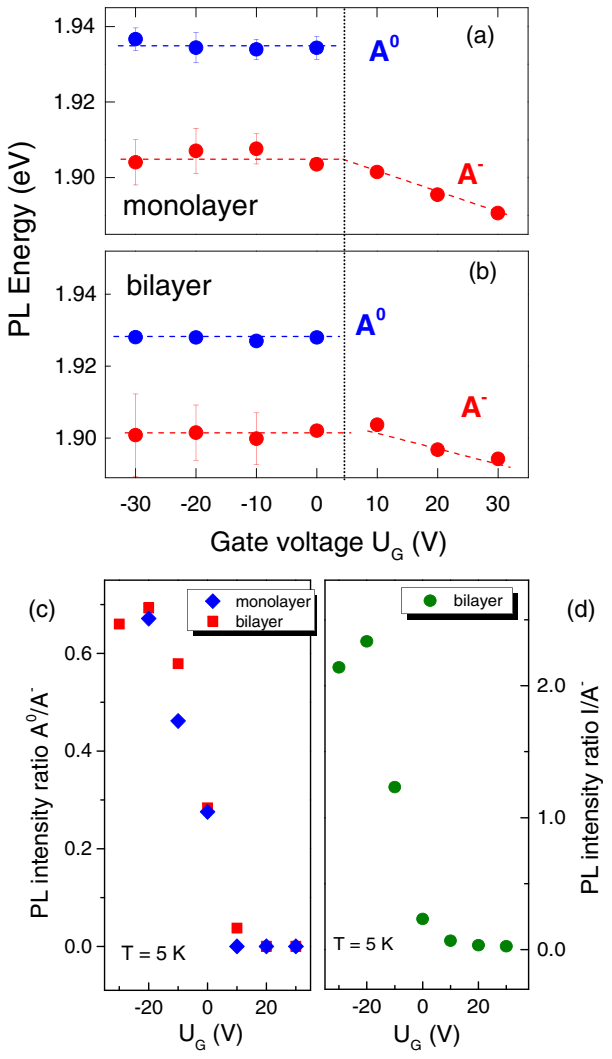

FIG. 4. (Color online) Gate-dependent photoluminescence: (a) and (b) PL energy for the excitonic and trionic emissions in the (a) monolayer and (b) bilayer structures. (c) PL Intensity ratio neutral/charged exciton for mono- and bilayers. (d) PL intensity ratio indirect (I)/direct (A^-) transition in the bilayer.

This statement is supported by the indirect transition. We do not observe any noticeable energy shift here as would be expected under an electric field [28,30]. Nevertheless, a switching behavior due to a change in the carrier population is apparent. This becomes clear when we depict the intensity ratio between exciton and trion for the A transition (A^0/A^- ratio) vs gate voltage U_G [Fig. 4(c)] and compare this with the ratio between the intensity of the indirect transition I and the PL intensity for the trion A^- (I/A^- ratio) as shown in Fig. 4(d). The dependence of the A^0/A^- ratio on U_G can directly be explained by the distinct switching from A^0 to A^- between $U_G = -10$ and 10 V that has been discussed already. The gate-voltage-dependent A^0/A^- intensity ratio is quite similar for mono- and bilayer devices. Interestingly, the I/A^- ratio in the bilayer device shows a very similar bias dependence as the A^0/A^- ratio. We therefore conclude that the switching between the I line and the A line is not due to electric fields but to the carrier redistribution within the bands: I and A^0 lines represent the dominating recombination channels for the electron depletion regime, whereas a change to a pure A^- recombination occurs for negatively charged MoS_2 bilayers, i.e., the accumulation regime.

Recently, stable trion emission even at room temperature has been reported for MoS_2 monolayer devices [26], which was attributed to the large trion binding energy in these two-dimensional crystals. In contrast, nothing is known about trion recombination in bilayers at elevated temperatures. As the trion binding energy is found to be similar in magnitude for both MoS_2 monolayers and bilayers, it is thus of great interest to figure out the consequence of the different band structures on the room-temperature trion emission in both devices.

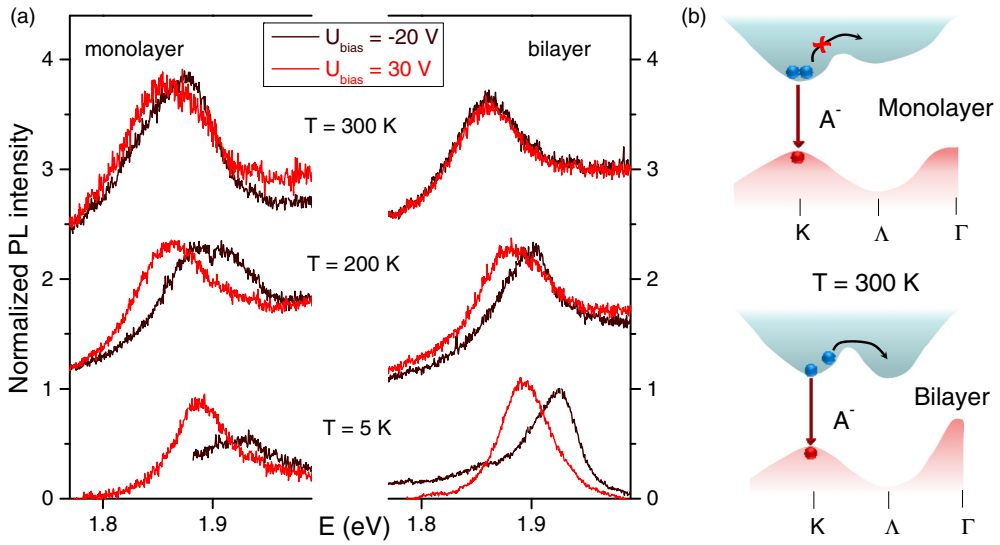

FIG. 5. (Color online) (a) Gate-voltage-dependent PL emission for monolayer MoS_2 (left) and bilayer MoS_2 (right) devices for different temperatures and two gate voltages in the depletion and accumulation regimes, respectively. (b) Sketch of the band structure illustrating possible trion dissociation in the bilayer at 300 K.

We measured the gate-dependent PL of the biased monolayer and bilayer devices at elevated temperatures. PL spectra at $U_G = -20$ and 30 V, respectively, are shown for $T = 5$, 200, and 300 K in Fig. 5(a). Obviously, the gate-controlled switching between trion and exciton is indeed possible for the MoS_2 monolayer device up to room temperature, in agreement with Ref. [26]. Surprisingly, the behavior is different for the bilayer: At $T = 5$ K the switching is much clearer here than for the monolayer device as discussed before, and the switching is still visible at $T = 200$ K. At room temperature, however, no bias dependence of the PL spectrum at all is obtained for the bilayer, in agreement with earlier findings [17]. Here we only record the neutral exciton line A^0, and no negative trions form even for $U_G = 30$ V, i.e., in the presence of large electron accumulation. These results can be easily understood by considering the band structure for monolayer and bilayer devices [Fig. 5(b)]: We propose that electrons can thermally escape the K-point valley much easier in bilayers due to the significantly lower conduction-band minimum at the Λ point in comparison with the monolayer samples. Thus, in the electron accumulation regime, the electrons are distributed between the K and the Λ points for the bilayer devices at room temperature, reducing the probability of trion emission from the K point, whereas they are kept confined in the K valley for the monolayer MoS_2.

IV. CONCLUSION

In conclusion, we could show that in electrically contacted MoS_2 flakes the carrier distribution in k-space can be controlled via gate voltage. Electron accumulation leads to distinct trionic emission, both in mono- and in bilayers with comparable trion binding energies. In contrast, under electron depletion conditions, the emission is dominated by neutral excitons, and additional recombination channels become present: In the case of the monolayer device, defect emission occurs whereas in bilayers, the indirect transition is enhanced. No signature of a field-induced Stark shift is found, whereas the observed energy shift in the accumulation regime is attributed to band-gap renormalization. In contrast to monolayers where trion emission is observed up to room temperature, the specific band structure of bilayers results in a thermal dissociation of trions at 200 K.

ACKNOWLEDGMENT

We thank O. Ochedowski and M. Schleberger for support in the Raman analysis of the MoS_2 flakes.

[1] Q. H. Wang, K. Kalantar-Zadeh, A. Kis, J. N. Coleman, and M. S. Strano, Nat. Nanotechnol. **7**, 699 (2012).
[2] K. F. Mak, C. Lee, J. Hone, J. Shan, and T. F. Heinz, Phys. Rev. Lett. **105**, 136805 (2010).
[3] W. J. Yu, Z. Li, H. Zhou, Y. Chen, Y. Wang, Y. Huang, and X. Duan, Nat. Mater. **12**, 246 (2013).
[4] J. S. Ross, P. Klement, A. M. Jones, N. J. Ghimire, J. Q. Yan, D. G. Mandrus, T. Taniguchi, K. Watanabe, K. Kitamura, W. Yao, D. H. Cobden, and X. D. Xu, Nat. Nanotechnol. **9**, 268 (2014).
[5] R. S. Sundaram, M. Engel, A. Lombardo, R. Krupke, A. C. Ferrari, P. Avouris, and M. Steiner, Nano Lett. **13**, 1416 (2013).
[6] B. W. H. Baugher, H. O. H. Churchill, Y. F. Yang, and P. Jarillo-Herrero, Nat. Nanotechnol. **9**, 262 (2014).
[7] K. Mak, K. He, J. Shan, and T. Heinz, Nat. Nanotechnol. **7**, 494 (2012).

[8] Y. L. Li, Y. Rao, K. F. Mak, Y. M. You, S. Y. Wang, C. R. Dean, and T. F. Heinz, Nano Lett. **13**, 3329 (2013).
[9] A. Splendiani, L. Sun, Y. Zhang, T. Li, J. Kim, C.-Y. Chim, G. Galli, and F. Wang, Nano Lett. **10**, 1271 (2010).
[10] E. S. Kadantsev and P. Hawrylak, Solid State Commun. **152**, 909 (2012).
[11] S. Wu, J. S. Ross, G.-B. Liu, G. Aivazian, A. Jones, Z. Fei, W. Zhu, D. Xiao, W. Yao, D. Cobden, and X. Xu, Nat. Phys. **9**, 149 (2013).
[12] G. Sallen, L. Bouet, X. Marie, G. Wang, C. R. Zhu, W. P. Han, Y. Lu, P. H. Tan, T. Amand, B. L. Liu, and B. Urbaszek, Phys. Rev. B **86**, 081301 (2012).
[13] J. S. Ross, S. Wu, H. Yu, N. J. Ghimire, A. M. Jones, G. Aivazian, J. Yan, D. G. Mandrus, D. Xiao, W. Yao, and X. Xu, Nat. Commun. **4**, 1474 (2013).
[14] H. Zeng, J. Dai, W. Yao, D. Xiao, and X. Cui, Nat. Nanotechnol. **7**, 490 (2012).
[15] A. M. Jones, H. Yu, J. S. Ross, P. Klement, N. J. Ghimire, J. Yan, D. G. Mandrus, W. Yao, and X. Xu, Nat. Phys. **10**, 130 (2014).
[16] S. Tongay, J. Zhou, C. Ataca, K. Lo, T. S. Matthews, J. Li, J. C. Grossman, and J. Wu, Nano Lett. **12**, 5576 (2012).
[17] A. K. M. Newaz, D. Prasai, J. I. Ziegler, D. Caudel, S. Robinson, R. F. Haglund, Jr., and K. I. Bolotin, Solid State Commun. **155**, 49 (2013).
[18] W. Jin, P.-C. Yeh, N. Zaki, D. Zhang, J. T. Sadowski, A. Al-Mahboob, A. M. van der Zande, D. A. Chenet, J. I. Dadap, I. P. Herman, P. Sutter, J. Hone, and R. M. Osgood, Jr., Phys. Rev. Lett. **111**, 106801 (2013).
[19] W. Zhao, R. M. Ribeiro, M. Toh, A. Carvalho, C. Kloc, A. H. Castro Neto, and G. Eda, Nano Lett. **13**, 5627 (2013).
[20] A. Castellanos-Gomez, R. Roldan, E. Cappelluti, M. Buscema, F. Guinea, H. S. J. van der Zant, and G. A. Steele, Nano Lett. **13**, 5361 (2013).
[21] A. Steinhoff, M. Roesner, F. Jahnke, T. O. Wehling, and C. Gies, Nano Lett. **14**, 3743 (2014).
[22] E. Cappelluti, R. Roldan, J. A. Silva-Guillen, P. Ordejon, and F. Guinea, Phys. Rev. B **88**, 075409 (2013).
[23] H. J. Conley, B. Wang, J. I. Ziegler, R. F. Haglund, Jr., S. T. Pantelides, and K. I. Bolotin, Nano Lett. **13**, 3626 (2013).
[24] Y. Yoon, K. Ganapathi, and S. Salahuddin, Nano Lett. **11**, 3768 (2011).
[25] B. Radisavljevic, A. Radenovic, J. Brivio, V. Giacometti, and A. Kis, Nat. Nanotechnol. **6**, 147 (2011).
[26] K. Mak, K. He, C. Lee, G. Lee, J. Hone, T. Heinz, and J. Shan, Nat. Mater. **12**, 207 (2013).
[27] E. Santos and E. Kaxiras, ACS Nano **7**, 10741 (2013).
[28] A. Ramasubramaniam, D. Naveh, and E. Towe, Phys. Rev. B **84**, 205325 (2011).
[29] Q. Liu, L. Li, Y. Li, Z. Gao, Z. Chen, and J. Lu, J. Phys. Chem. C **116**, 21556 (2012).
[30] Z. Zhang, M. Si, Y. Wang, X. Gao, D. Sung, S. Hong, and J. He, J. Chem. Phys. **140**, 174707 (2014).
[31] P. Tonndorf, R. Schmidt, P. Boettger, X. Zhang, J. Boerner, A. Liebig, M. Albrecht, C. Kloc, O. Gordan, D. R. T. Zahn, S. M. de Vasconcellos, and R. Bratschitsch, Opt. Express **21**, 4908 (2013).
[32] N. Scheuschner, O. Ochedowski, M. Schleberger, and J. Maultzsch, Phys. Status Solidi B **249**, 2644 (2012).
[33] D. Sercombe, S. Schwarz, O. Del Pozo-Zamudio, F. Liu, B. J. Robinson, E. A. Chekhovich, I. I. Tartakovskii, O. Kolosov, and A. I. Tartakovskii, Sci. Rep. **3**, 3489 (2013).
[34] G. Plechinger, F. X. Schrettenbrunner, J. Eroms, D. Weiss, C. Schueller, and T. Korn, Phys. Status Solidi RRL **6**, 126 (2012).
[35] T. C. Berkelbach, M. S. Hybertsen, and D. R. Reichman, Phys. Rev. B **88**, 045318 (2013).
[36] P. Cudazzo, I. V. Tokatly, and A. Rubio, Phys. Rev. B **84**, 085406 (2011).
[37] C. J. Zhang, H. N. Wang, W. M. Chan, C. Manolatou, and F. Rana, Phys. Rev. B **89**, 205436 (2014).
[38] Y. Li, C. Xu, B. Zhang, and L. Zhen, Appl. Phys. Lett. **103**, 033122 (2013).
[39] A. M. Jones, H. Yu, N. J. Ghimire, S. Wu, G. Aivazian, J. S. Ross, B. Zhao, J. Yan, D. G. Mandrus, D. Xiao, W. Yao, and X. Xu, Nat. Nanotechnol. **8**, 634 (2013).
[40] S. Tongay, J. Suh, C. Ataca, W. Fan, A. Luce, J. S. Kang, J. Liu, C. Ko, R. Raghunathanan, J. Zhou, F. Ogletree, J. Li, J. C. Grossman, and J. Wu, Sci. Rep. **3**, 2657 (2013).
[41] T. Cheiwchanchamnangij and W. Lambrecht, Phys. Rev. B **85**, 205302 (2012).